Sustainable Materials and Technologies 33 (2022) e00473

Contents lists available at ScienceDirect

Sustainable Materials and Technologies

journal homepage: www.elsevier.com/locate/susmat

Hydrothermally-assisted recovery of Yttria- stabilized zirconia (YSZ) from end-of-life solid oxide cells

Sofia Saffirio [a], Sergii Pylypko [b], Sabina Fiorot [c], Ilaria Schiavi [c], Silvia Fiore [d], Massimo Santarelli [e], Domenico Ferrero [e], Federico Smeacetto [a], Sonia Fiorilli [a,*]

[a] Department of Applied Science and Technology, Politecnico di Torino, C.so Duca degli Abruzzi 24, 10129 Torino, Italy
[b] Elcogen, Valukoja 23, 11415 Tallinn, Estonia
[c] Environment Park S.p.A., Via Livorno 60, 10144 Torino, Italy
[d] Department of Environment, Land, and Infrastructure Engineering, Politecnico di Torino, C.so Duca degli Abruzzi 24, 10129 Turin, Italy
[e] Department of Energy, Politecnico di Torino, C.so Duca degli Abruzzi 24, 10129 Torino, Italy

ARTICLE INFO

Keywords:
Solid oxide cell
End-of-life
Yttria-stabilized zirconia (YSZ)
Recovery
Hydrothermal treatment
Selective Ni leaching

ABSTRACT

Effective and scalable recycling strategies for the recovery of critical raw materials are yet to be validated for solid oxide cells (SOCs) technologies. The current study aimed at filling this gap by developing optimized recycling processes for the recovery of Yttria-stabilized Zirconia (YSZ) from End-of-Life (EoL) SOC components, in view of using the recovered ceramic phase in cell re-manufacturing. A multi-step procedure, including milling, hydrothermal treatment (HT), and acidic-assisted leaching of nickel from composite Ni-YSZ materials, has been implemented to obtain recovered YSZ powders with defined specifications, in terms of particle size distribution, specific surface area, and chemical purity. The overall optimized procedure includes a pre-milling step (6 h) of the EoL composite materials, and a hydrothermal (HT) treatment at 200 °C for 4 h to further disaggregate the sintered composite, followed by selective oxidative leaching of Ni^{2+} by HNO_3 solution at 80 °C for 2 h. In particular, the intermediate HT step was assessed to play an essential role in promoting the disaggregation of the sintered powders, with a related increase of specific surface area (up to 13 $m^2\ g^{-1}$) and the overall reduction of the primary particle aggregates. The acid-assisted leaching allowed to fully extract Nickel from the composite Ni-YSZ powders, with retention of YSZ crystallinity and negligible loss of Zr and Y, as revealed by ICP analysis on the recovered supernatants.

The developed multi-step pathway offers a promising strategy to recover valuable YSZ materials for the re-manufacturing of SOCs components, with the aim to boost a circular economy approach in the field of fuel-cell and hydrogen (FCH) technologies.

1. Introduction

Climate change is one of the most critical issues of our time, and the overdependence on environmentally hazardous approaches by both industry and society requires an urgent action to reduce the impact of human activities and, in line with the Paris Agreement objective, to keep the global temperature increase to well below 2 °C (Paris Agreement, United Nations, 2015). Within this framework, the European Green Deal (The European Green Deal, European Commission, 2019) sets the foundation for a series of advanced energy policies and long-term strategies, defined in the New Circular Economy Action Plan (New Circular Economy Action Plan, European Commission, 2020), that aims to achieve a carbon-neutral EU with zero-net greenhouse gas (GHG) emissions by 2050.

Within this framework, FCH (Fuel-Cell and Hydrogen) technologies play a crucial role in the transition towards decarbonization, being hydrogen an energy vector that allows for local energy storage, electricity generation, heat recovery, balancing of renewable electricity production and transport [1]. Among FCH solutions, solid oxide fuel cells (SOFCs) and solid oxide electrolyser cells (SOECs) are jointly referred to as solid oxide cells (SOCs). In particular, SOFCs offer an efficient, fuel-flexible, and environmentally friendly technology [2] for electricity production, as an alternative to fossil fuel combustion, while SOECs offer an enhanced efficiency in water splitting to hydrogen (H_2)

* Corresponding author.
E-mail address: sonia.fiorilli@polito.it (S. Fiorilli).

https://doi.org/10.1016/j.susmat.2022.e00473
Received 6 May 2022; Received in revised form 8 July 2022; Accepted 29 July 2022
Available online 2 August 2022

		Incorporated YSZ Electrolyte, global	Incorporated YSZ Anode, global	Incorporated Ni Anode, global
	GW, global	tonn	tonn	tonn
2024	Low: 6.88	138	3000	2400
	High: 25.12	502	11000	9000
2030	Low: 6.88	370	8000	6500
	High: 25.12	2032	43700	35600

Fig. 1. Expectations for the demand of Ni and YSZ for FCH applications.

and oxygen (O_2). However, despite the significant advancements achieved in the last two decades, some major challenges in the field of SOCs technologies are still unmet and require to be addressed in order to achieve their market breakthrough, especially in terms of life-cycle costs [3].

The full deployment of SOCs is further hindered by the lack of efficient, scalable and cost-effective end-of-life (EoL) strategies [4], enabling the management and valorisation of waste products derived from stacks operation and avoiding their landfills disposal. For a technology to be entirely sustainable, in fact, waste management is as essential as the development and application, since a reduced consumption of virgin materials would also minimize the environmental impact of the production stage [5].

SOCs consist of a dense oxygen-ion conducting electrolyte interposed between two porous electrodes that enable gas permeation [6]. The electrolyte can be structurally supported on either the anode or cathode component (anode-supported [7] or cathode-supported [8] cell, respectively, referring to SOFCs), or it can act as a structural component itself (electrolyte-supported cell) [9]. State-of-the-art materials mostly used in SOCs systems are YSZ (Yttria-stabilized Zirconia) as the electrolyte [10], LSM/LSC (Strontium-doped Lanthanum Manganite/Cobaltite) as the oxygen electrode [11,12] and NiO-YSZ cermet as the fuel electrode [13], which undergoes reduction to Ni-YSZ during SOFC operation.

As mentioned before, EoL strategies specifically conceived and implemented for the recovery and reuse of critical and hazardous materials from exhausted SOCs are almost absent. A recent comprehensive study by Valente et al. [4] reviewed the overall existing and novel technologies for the recovery of valuable materials from FCH products, including Ni, YSZ and LSC, and concluded that no EoL processes are currently available for SOCs components. Similarly, Férriz et al. [14] pointed out the need of addressing EoL recycling perspectives for hydrogen technologies, and provided an overall classification of FCH materials based on related hazardousness, scarcity and cost. According to this classification, suitable recovery strategies for SOCs should be explored not only for Ni and LSC as critical raw materials, but also for YSZ, due to its related high economic value. The most common SOC cells are constituted of roughly 90% by weight of YSZ and NiO (50/50 for NiO/YSZ), thus the recycling of these two components would translate into related cost-saving for manufactures and would mitigate the criticality of supply on the global market, paving the way for a growing FCH market.

According to the E4tech report [15] focused on the study of the value chain and manufacturing competitiveness for Hydrogen and Fuel Cells Technologies, the expectation of Ni and YSZ for FCH applications can be estimated as illustrated below (Fig. 1).

These are significant additions to the existing requirements of the industry, also considering that a few of the above materials are required in growing market, from electronics to batteries for electric vehicles.

In a recent study by Mori et al. [16], the three evaluation criteria (hazardousness, scarcity and cost) have been merged into a single score for a preliminary evaluation of the life cycle impact (LCI) of materials used in the most mature FCH technologies using a life-cycle assessment (LCA) approach. Since most of SOC components are still in their development stage, the call for a combined effort from the FCH industrial sector and research institutions to implement current LCI databases – including materials, their mass ratios in FCH technologies, exact production processes, followed by end-of-life scenarios– clearly emerged as a crucial need from this study.

At this stage, given the lack of well-established technologies for EoL SOCs, recycling solutions can be adapted from other industrial sectors, where the recovery of RREs (Rare-Earth Elements) and valuable metals has been widely investigated for e-wastes, spent batteries, and spent catalysts starting from the metallurgical processes used for the extraction of metals from ores [17]. The most common recovery strategies for critical raw materials, including Ni, Co and La among others, are based on the stirring/ultrasound-assisted leaching by using inorganic acids such as HNO_3, HCl and H_2SO_4 [18–27], at concentrations of about 1–2.5 M and temperatures in the range of 60–80 °C for 1–6 h, achieving >95% extraction efficiency in most cases.

With the purpose of contributing to the definition of ad hoc EoL strategies for SOCs, the present study focuses on the implementation of a multi-step process aimed at recovering the YSZ phase of Ni-YSZ composite materials from end-of-life (EoL) cells, dismantled from stacks after long-time operation (*ca* 10,000 h).

The recycling procedure has been developed by combining and adapting established hydrometallurgical methods, primarily consisting of metal leaching by using inorganic acids, with a pre-treatment based on hydrothermal (HT) technologies to enhance the disaggregation and pulverization of sintered composite materials and the subsequent metal leaching. In particular the selection of HT-assisted recycling strategy has been inspired by the work of Kamiya et al. [28] focusing on the disintegration of pure YSZ-based sintered ceramics into powdery particles, aiming at their recycling to re-manufacture dense sintered bodies.

The overall recovery pathway is schematically outlined in Fig. 2 and includes the detachment of top LSC layer, sequential milling and HT treatments in order to disaggregate and pulverize the sintered cermet components, followed by an oxidative selective leaching of Ni to recover

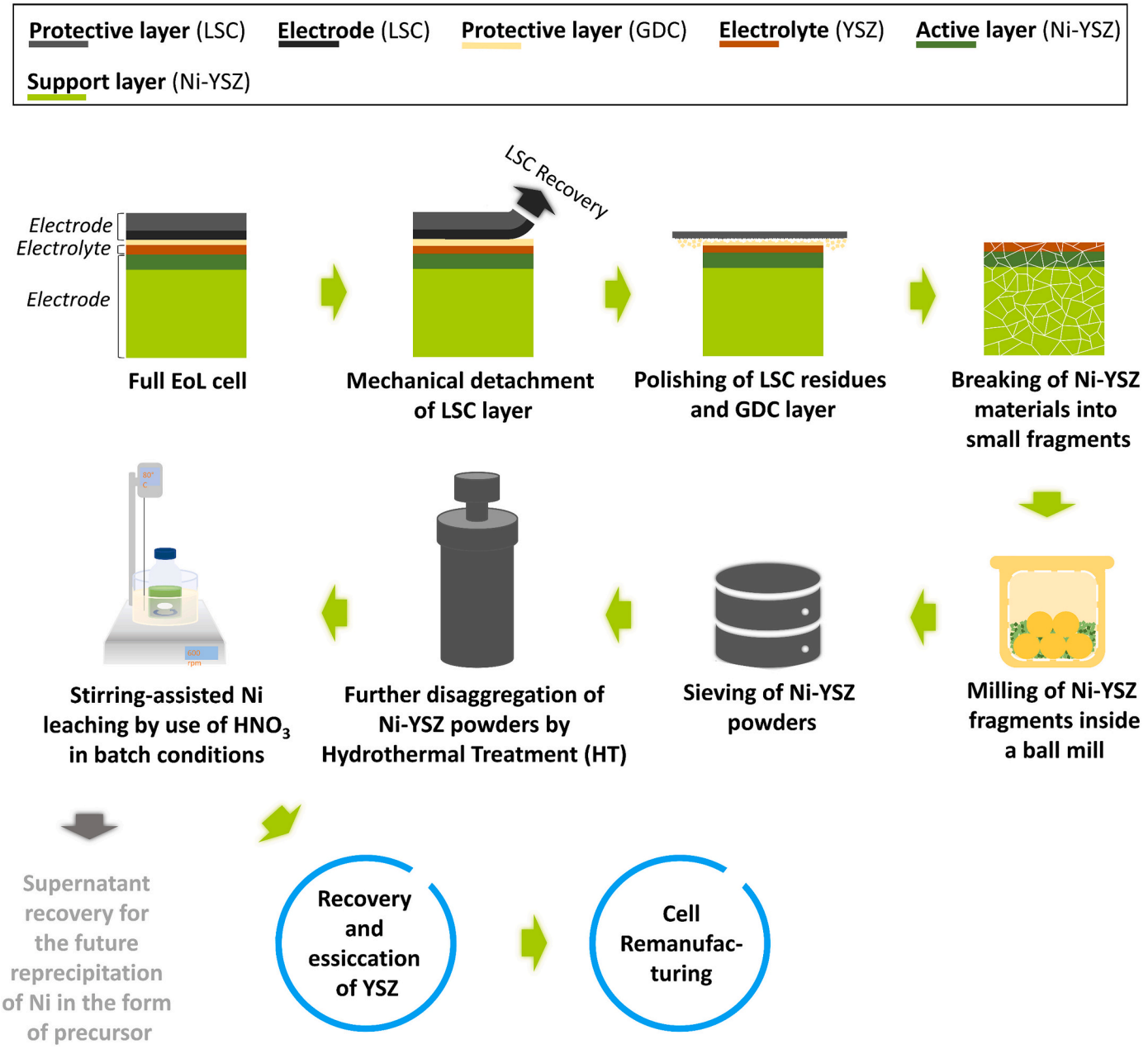

Fig. 2. Schematic outline of the followed pathway for the recovery of YSZ from EoL SOCs.

the YSZ phase.

Given the ultimate purpose of re-using the recovered YSZ for cell manufacturing, according to the manufacturer specifications some acceptance criteria must be targeted by the recycled powders, concerning the particle size distribution, specific surface area and chemical purity. Therefore, an extensive physico-chemical characterization of the powders after each step has been conducted to define the most efficient process in terms of milling time and HT conditions (i.e. duration, temperature) and to guarantee the best combination in terms of recovery yield and overall energy/chemicals consumption.

2. Materials and methods

2.1. Multi-step recovery procedure for EoL SOCs

EoL cells were provided by Elcogen (Elcogen AS, Tallin, Estonia) after dismantling from SOC stacks. As schematically reported in Fig. 1, cells are composed from the bottom by a 300 μm thick NiO-YSZ (reduced to Ni-YSZ during cell operation) electrode, 3-6 μm thick YSZ (8% mol. Y, 8YSZ) electrolyte, GDC (Gadolinium-doped Ceria) protective layer and 12 ± 5 μm-thick LSC top layer electrode (https://elcogen.com/). The Ni-YSZ (3% mol. Y, 3YSZ) composite layers represent the major component of the considered cell, constituting its 95% wt., and it will be the focus of the recovery pathway outlined in this study.

Given the as-received EoL cells, the top LSC layer was detached through mechanical scratching by use of a metallic spatula, to separate the bottom cell components. The GCD layer, together with some LSC residues, was instead removed by using 600 and 800 grit polishing papers on a rotating polisher (Struers, LaboPol-2) provided with water stream. The resulting half cells were then crushed into pieces of few cm^2 and subsequently milled to reduce the size of the Ni-YSZ materials and increase the exposed specific surface area (SSA). Specifically, a 250 ml zirconia grinding bowl (Fritsch), provided with 6 grinding balls with 30 mm diameter, was placed into a planetary mono mill (FritschTM,

a)

EDS Elemental Analysis

Before polishing		After polishing	
Element Symbol	Atomic Conc. (%)	Element Symbol	Atomic Conc. (%)
O	58.77	O	27.06
Ce	**10.47**	**Ce**	**ND**
Gd	**3.69**	**Gd**	**ND**
Sr	**3.12**	**Sr**	**ND**
Zr	14.30	Zr	17.36
Ni	6.90	Ni	52.78
Y	2.16	Y	1.51

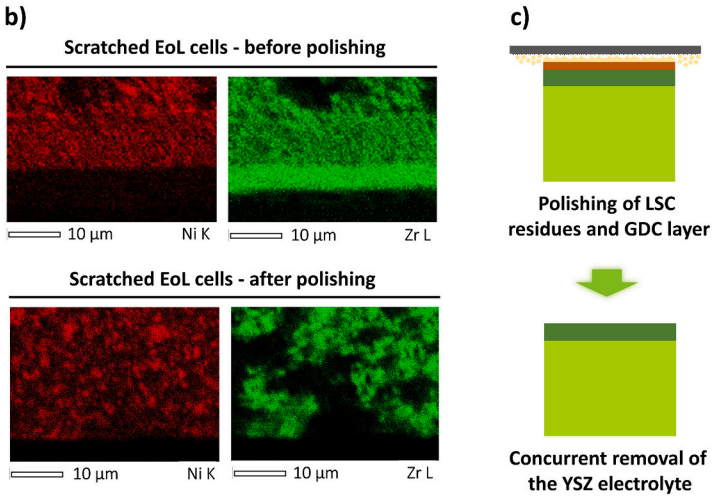

Fig. 3. (a) EDS elemental analysis carried out on scratched EoL cells before (left) and after (right) polishing, showing the complete removal of contaminants from the Ni-YSZ materials underneath; (b) EDS mapping of Ni (red) and Zr (green) elements on scratched EoL cells before (above) and after (below) polishing and (c) schematic representation (reference to Fig. 2) of the concurrent removal of dense electrolyte layer.

Pulverisette 6 Planetary Mono Mill) and run at 450 rpm for 6 h at this purpose. The resulting Ni-YSZ powders were sieved under 25 µm by using a vibrating sieving machine (Endecotts, Octagon 200 Sieve Shaker) for 60 mins. Sieved powders were subjected to hydrothermal (HT) treatment in order to induce their further aggregation/pulverization and to facilitate the subsequent Ni extraction. In particular, HT was carried out at 200 °C in a static stainless-steel reactor (Berghof, Pressure Digestion Vessel DAB-3) filled with 100 ml of water (50% of the total reactor volume) and 2 g of milled Ni-YSZ material, at increasing treatment times (1 h, 2 h, 4 h, 12 h). Acid-assisted Ni extraction was then performed by contacting HT-treated powders with HNO_3 (Sigma Aldrich, ≥65%) aqueous solution 2.2 M (1:50 solid to liquid ratio) at 80 °C for 2 h, while stirring the resulting suspension at 600 rpm. In particular, the HNO_3-assisted treatment of Ni-YSZ reported by Kim et al. [29] has been used as starting point and adapted to the specific purposes of the study. The resulting supernatants were filtered by means of a 0.22 µm syringe filter and stored at 4 °C for further analysis of extracted Ni concentration. The recovered YSZ powders were instead subjected to multiple washing and centrifugation steps, performed at 10′000 rpm for 5 mins each, before drying at 60 °C overnight for the recovery and characterization.

2.2. Characterization

The efficacy of the polishing step on removing the GDC layer and LSC residues was assessed by Energy-dispersive X-Ray Spectroscopy (EDS, Jeol, EX-37001) on the cell components, in high vacuum conditions and at a voltage of 15 kV. EDS analyses were also performed -at the final stage of the recovery process- on the powders resulting from acidic Ni leaching to provide a semiquantitative evaluation of Ni extraction.

The crystalline structure of powders before and after milling, HT treatment and acid leaching, was examined by X-Ray Diffraction (XRD, Panalytical, Xpert3 MRD) analysis using Cu Kα radiation at a voltage of 40 kV and a current of 40 mA, to evaluate any possible structural change or degradation induced by each step of the process. The XRD patterns were collected in the 2θ range of 10–70°.

N_2 adsorption-desorption isotherm analyses were conducted by using an ASAP2020 Micromeritics analyser at a temperature of −196 °C, after degassing the powders at 150 °C for 4 h, to evaluate the specific surface area (SSA) after milling and HT treatment for increasing times. The Brunauer–Emmett–Teller (BET) equation was used to calculate the specific surface area (SSA_{BET}) from the adsorption isotherm in the 0.04–0.2 relative pressure range.

The same powders were also analysed through with a Zetasizer nano ZS90 (Malvern Instruments Ltd., Malvern, UK) at RT to assess their average particle size distribution (PSD) after the milling and HT steps. The preparation consisted to disperse 3 mg of powders in 3 mL of ddH2O, containing DARVAN as dispersing agent (2.5% vol.), to obtain a concentration of 1 mg/mL and sonicate for 10 min.

Field Emission Scanning Electron Microscopy (FESEM, Jeol, JCM-6000Plus, Benchtop SEM) was instead performed in high vacuum conditions and at a voltage of 5 kV to evaluate the morphological features of the powders after the milling, HT, acidic leaching and sintering treatment.

The concentration of Ni, Y and Zr in the supernatants recovered after acidic leaching was measured by Inductively Coupled Plasma Atomic Emission Spectrometry Technique (ICP-AES) (ICP-MS, Thermoscientific, Waltham, MA, USA, ICAP Q), after appropriate dilutions, to evaluate the Ni extraction efficiencies [30] and the potential degradation of the ceramic phase.

3. Results and discussion

3.1. LSC layer detachment and polishing step

Considering the structure of the considered SOCs (Fig. 2), the removal of the LSC electrode and GDC protective layer is the first step required to isolate the bottom YSZ electrolyte and Ni-YSZ composite electrode for the subsequent recovery operations. Due to the fragile nature of the cells, this step was carried out through manual mechanical scratching. In particular, the detachment was conducted while keeping the cell immersed in water, since this approach proved to improve the efficacy of this initial step, enabling to reduce significantly the residues of the LSC layer.

However, the conducted mechanical scratching was found to be ineffective towards the removal of the GDC protective layer (Fig. 3) underneath, which remained deposited on top of the electrolyte and which is undesirable for the recovery of the materials of interest, namely Ni and YSZ. As a consequence, an additional polishing step was added to the process in order to remove any possible contaminants that might compromise the recovery of a high-purity ceramic phase from the electrolyte and Ni-YSZ electrode.

EDS analysis allowed to assess the presence of elements - other than nickel, yttrium and zirconium - on the scratched cell before and after polishing. Results are shown in Fig. 3.a, where gadolinium and cerium elements, along with some strontium residues from the LSC scratched

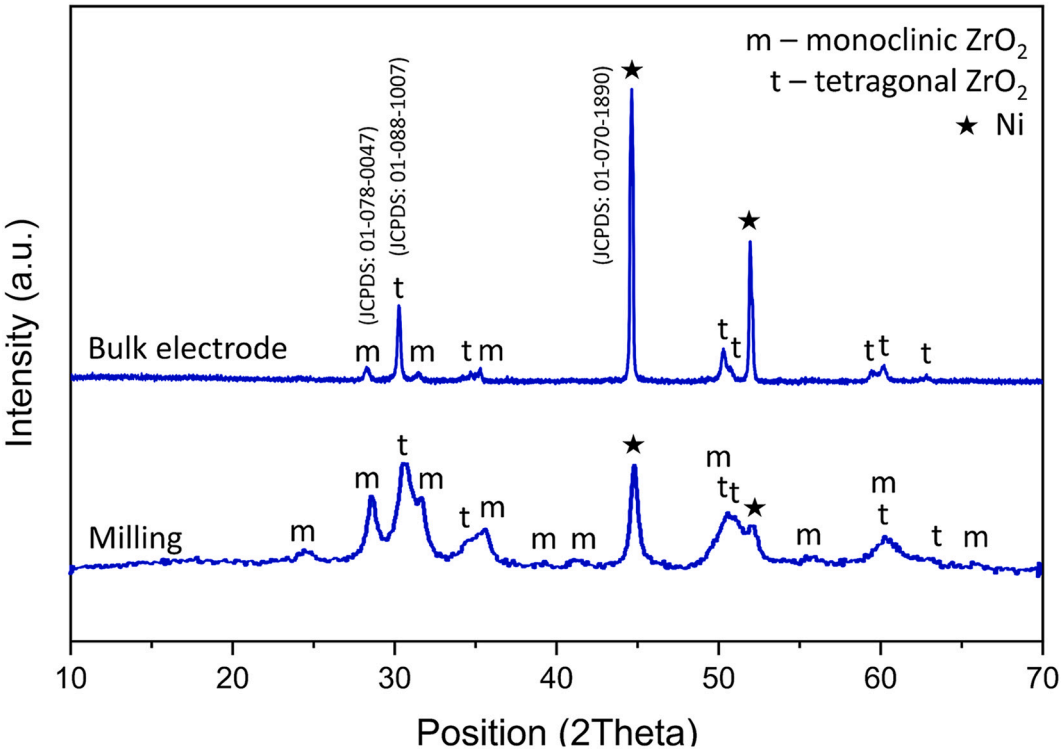

Fig. 4. XRD spectra of Ni-YSZ composite electrode from EoL SOCs before and after milling for 6 h. The patterns of tetragonal and monoclinic YSZ are provided below as reference patterns.

electrode before polishing, are evidenced. No traces of residual contaminants were instead detected after the polishing step, which was therefore demonstrated to be effective in terms of complete removal of the top electrode and the GDC protective layer.

Since manual polishing does not enable a precise control on the thickness of the removed layers, further investigations have been performed, in order to get deeper insights regarding the possible concurrent massive asportation of the YSZ electrolyte and Ni-YSZ electrode. In particular, by exploiting the different compositions and densities of the YSZ electrolyte and Ni-YSZ electrode, a comparison of EDS elemental mapping of Ni and Zr was carried out on the electrolyte side of scratched EoL cells before and after polishing. Results in Fig. 3.b show the complete asportation of the dense YSZ electrolyte, along with the low-porous Ni-YSZ active layer of the electrode. The removal of these two layers both containing YSZ 8% mol of yttrium (8YSZ) is also evidenced by a decrease of Y/Zr ratio, as shown in Fig. 3 (a), since after polishing the residual support contains exclusively YSZ with 3% mol. of yttrium (3YSZ).

However, being the high-porous Ni-YSZ electrode the major component of the cell, accounting for >90% of its thickness, the extent of the loss was not considered an issue in terms of the overall recovery yield. The Ni-YSZ composite electrode is thus the focus of the recovery process that will be outlined step-by-step throughout this study.

3.2. *Effect of milling*

Milling is an essential step to reduce the cells into powders and to enhance the surface area that is directly exposed to the acid leaching for Ni extraction. For this reason, milling was performed on the fragmented Ni-YSZ materials and optimized in order to induce their effective pulverization, while still preserving the crystallinity of the ceramic phase. In particular, a milling time of 6 h was selected as a result of preliminary investigations, since this duration allowed the best outcomes in terms of SSA increase and retention of crystalline structure. Longer milling duration times did not provide significant improvements and were thus discarded based on energy-consumption considerations.

XRD spectra were recorded for Ni-YSZ material both as bulk electrode (after the detachment of the top layer) and as powders resulting

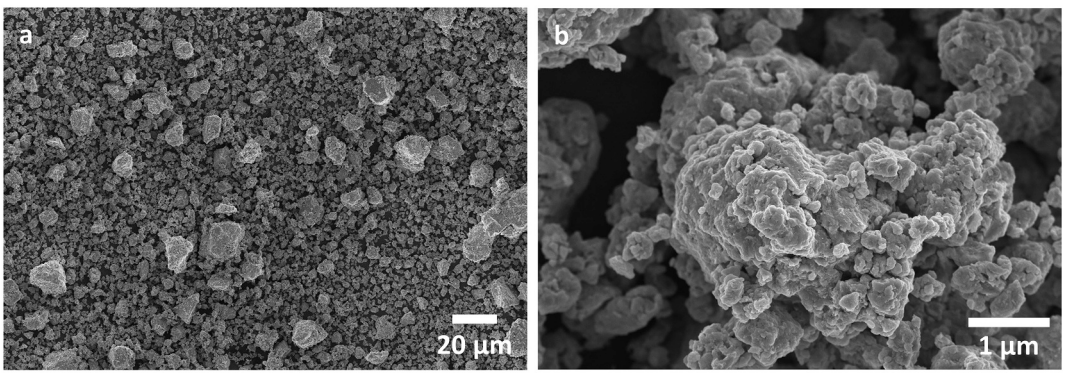

Fig. 5. FE-SEM images of Ni-YSZ powders after 6 h milling.

Table 1
Specific surface area (SSA) and Particle Size Distribution (PSD) of EoL Ni-YSZ powders after milling for 6 h.

Treatment	Specific Surface Area ($m^2\ g^{-1}$)	Particle Size ± Std. Dev. * (nm)
Milling 6 h/sieving below 25 μm	8	400 ± 80

* Derived from distribution % number.

from 6 h milling, leading to the diffraction patterns shown in Fig. 4. The reflections for each of the corresponding crystalline phases are indicated above the diffraction peaks: as expected, the main phase is YSZ, both in its tetragonal (JCPDS 01–088-1007; major reflections at 30.224°, 50.221° and 60.203°) and monoclinic (JCPDS 01–078-0047; major reflections at 28.192°, 31.467° and 24.068°) crystalline structures. Metallic Ni (JCPDS 00–070-1890 with peaks at 44.508°, 51.847° and 76.372°) was also detected. It is noteworthy to highlight that, as reported in detail by Götsch et al. [31], the tetragonal and cubic diffractograms of YSZ can be hardly distinguished as the two polymorphs feature lattice planes with the same spacing.

The pattern of the milled powder evidences a significant transformation of the metastable tetragonal phase into the monoclinic phase, accompanied by a large volume increase and the consequent spontaneous disintegration of the sintered body due to microcracking propagation under the particle surface. A significant broadening of the diffraction peaks is due to the overall decrease of the crystallites size, which results from the pulverization of grains from the bulk electrodes into powder particles smaller in size.

In particular, FESEM micrographs of powders after milling and sieving below 25 (Fig. 5) reveal mostly micro and sub-microparticles, with few larger aggregates of about 10–20 μm. The particle size distribution was evaluated through DLS analysis (average of 3 measurements), which revealed distribution (% number) centred at around 400 nm, with a smaller contribution of particles aggregates (see Table 1).

The presence of residual microsized aggregates is clearly evidenced by the particle size distribution reported as % volume, which revealed a multimodal distribution with two major peaks at values >1 μm (Fig. S1 (a) in the Supplementary Information section).

The N_2 adsorption-desorption analysis on milled and sieved powders revealed a value of SSA_{BET} (Table 1) of around 8 $m^2\ g^{-1}$.

The characterization carried out on the powders after the milling step is considered as a starting reference to highlight the transformations induced by the following steps of the recovery process.

3.3. Effect of HT treatment

As mentioned in Section 3.2, the milled powders consist of primary sub-microparticles and micrometric aggregates with limited overall surface exposition, a key aspect to be targeted for an effective leaching of the metallic phase from the Ni-YSZ composite. To this final purpose, the combination of temperatures in the range of 200–300 °C and pressure in the range of 20–30 MPa [32,33] was exploited in the attempt to further disaggregate Ni-YSZ powders and increase their specific surface area to maximize the accessibility of the acidic medium to the Nickel embedded into the ceramic phase. To the best of our knowledge, no previous studies explored the exploitation of HT treatment for the specific purpose of disaggregating Ni-YSZ composite materials dismantled from EoL SOCs. In the literature, only two contributions [28,34] focusing on the disintegration of sintered YSZ bodies into powdery particles have been found, and the reported operating conditions have been adapted for the composite Ni-YSZ powder under investigation with the aim to implement a specific recycling process.

For a given temperature fixed at 200 °C, the effect of increasing treatment times (2 h, 4 h, 12 h) on the crystalline structure, SSA and PSD values, and on the possible leaching of elements due to degradation of the ceramic phase have been investigated. The overall set of obtained results is reported in Fig. S1 (a), Fig. S2 and Table S1 in the Supplementary Information section. Based on this investigation, the optimal treatment time resulted in 4 h, as longer duration times (up to 12 h) did not provide substantial benefits in terms of specific surface area and decrease of average particle size. XRD of hydrothermally treated powder (Fig. 6) did not reveal any remarkable variation in the crystallinity of the ceramic phase, except for a slight further increase of the percentage of

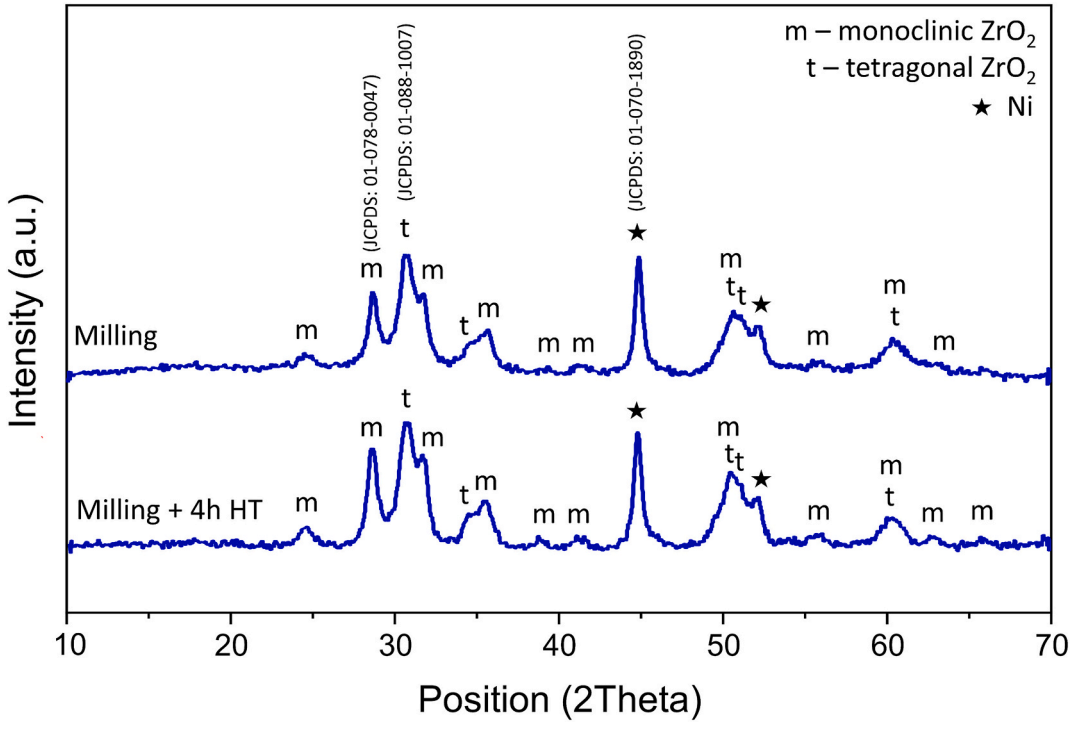

Fig. 6. XRD spectra of EoL Ni-YSZ materials milled and subsequently hydrothermally-treated at 200 °C for 4 h to induce the disaggregation of YSZ.

Table 2
SSA of EoL Ni-YSZ powders after HT treatment at 200 °C and 4 h, and concentrations of leached Ni, Y and Zr evaluated by ICP analysis on the supernatants recovered after HT treatment.

Treatment	Specific Surface Area ($m^2\ g^{-1}$)	ICP Elemental analysis (ppm)		
		Ni	Y	Zr
Milling +4 h HT	13	0.6	ND*	ND*

* ND: not detectable.

the monocline phase.

At variance SSA (Table 2.a) resulted significantly affected by the HT treatment, increasing up to 13 $m^2\ g^{-1}$ compared to 8 $m^2\ g^{-1}$ of the powder after milling.

The observed increase of exposed surface area (Table 2), compared to the powder after milling, is directly ascribed to the disaggregation of the sintered ceramic powders and, to a lower extent, to the local surface reactivity promoted by the hydrothermal conditions (i.e. surface hydroxylation). As mentioned before, by increasing the treatment time up to 12 h, SSA did not undergo significant improvement, showing the same values as reported for 4 h treatment. PSD distribution expressed as % number did not reveal any substantial change after HT treatment (Table S1), evidencing a monomodal peak centred at around 400 nm, in analogy to that reported for milled powders. On the contrary, the PSD expressed as % volume (more sensitive to the presence of aggregates) evidenced a clear reduction of the peaks ascribed to micro-sized particle aggregates (Fig. S1 (b)), suggesting an overall reduction in comparison with the milled powders (Fig. S1 (a)).

Table 2 also reports the concentrations for Ni, Y and Zr elements revealed by ICP analysis carried out on the supernatants retrieved after the HT treatments at increasing treatment times. Despite a slight increase in the amount of leached-out Ni for longer treatment durations, the overall extent of leaching can be considered negligible, as only 0.6 ppm of Ni were detected in the supernatant after 4 h of treatment. The analysis also confirmed that the YSZ ceramic phase was fully preserved, since no leaching of Zr and Y was observed at any treatment time.

FESEM micrographs of the powders before and after hydrothermal treatment under the optimized HT conditions are shown in Fig. 7, which clearly evidences, both at low and high magnification, the positive disaggregation effect induced by HT on the Ni-YSZ composite powders, in terms of significant reduction of large aggregates and disaggregation of sintered primary particles. In accordance to the results reported for pure sintered YSZ body, the disaggregation effect mostly derives from a further tetragonal to monocline phase transformation, associate to volume increase and microcrack propagation [4,28], and to the occurrence of hydrolysis of the ceramic framework at the grain boundaries promoted by the hydrothermal conditions.

3.4. Acidic-assisted Ni-leaching from HT-treated Ni-YSZ powders

The following step of the recovering route consisted in the selective extraction of Ni from the composite material through acid-assisted leaching, with the aim to recover YSZ powders. The extraction by HNO_3 solution was carried out according to the experimental conditions defined in Paragraph 2.1, through a stirring-assisted batch process carried out at 80 °C. The occurrence of Ni extraction resulted confirmed by a visual inspection of the acid-treated material, as shown in Fig. 8, whose bleaching was clearly assessed by a comparison with milled and HT-treated powders.

The XRD diffractograms before and after the acid leaching reported in Fig. 9 confirm the removal of the metallic phase, witnessed by the disappearance of the main peaks associated to metallic nickel.

The leaching efficacy was further confirmed by the ICP results reported in Table 3.a, where the value of Ni^{2+} concentration for the supernatants recovered after acid treatment exhibited - as expected - a drastic increase (8×10^3 ppm) compared to the value registered on supernatant collected after HT treatment (0.6 ppm). A concurrent massive decrease in the amount of residual Ni, from 20.7 to 0.8 mol%, was registered by EDS analysis on powders before and after acid leaching, respectively. Although EDS analysis provides semiquantitative compositions, the residual 0.8% atomic percentage of Ni detected on leached powder can be considered as reliable evidence that almost the

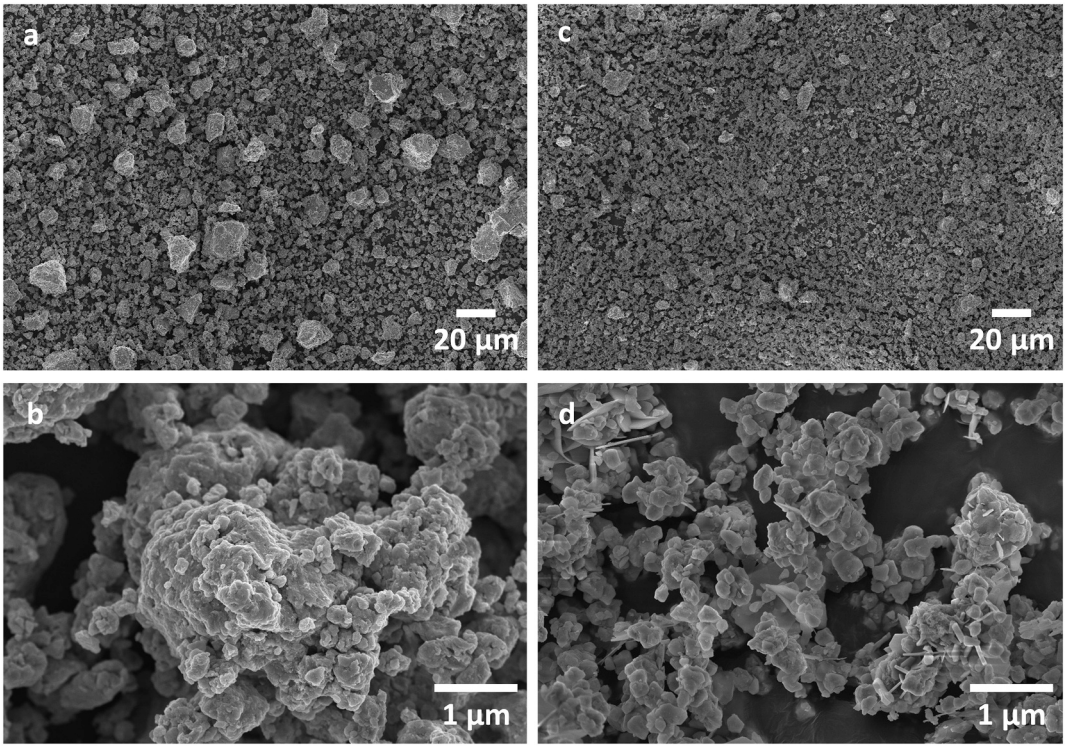

Fig. 7. FESEM morphological characterization of EoL Ni-YSZ powders before (a,b) and after (c,d) undergoing HT disaggregation under the optimized conditions.

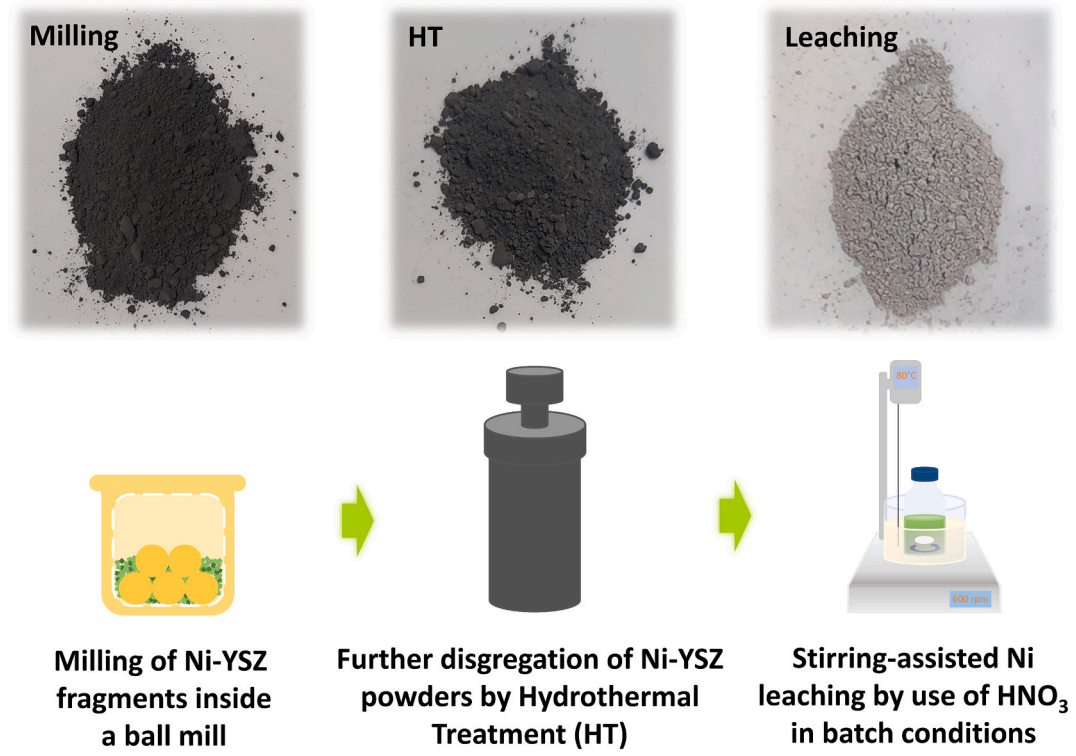

Fig. 8. Pictures showing the bleaching of Ni-YSZ powders after selective extraction of nickel by HNO_3 leaching.

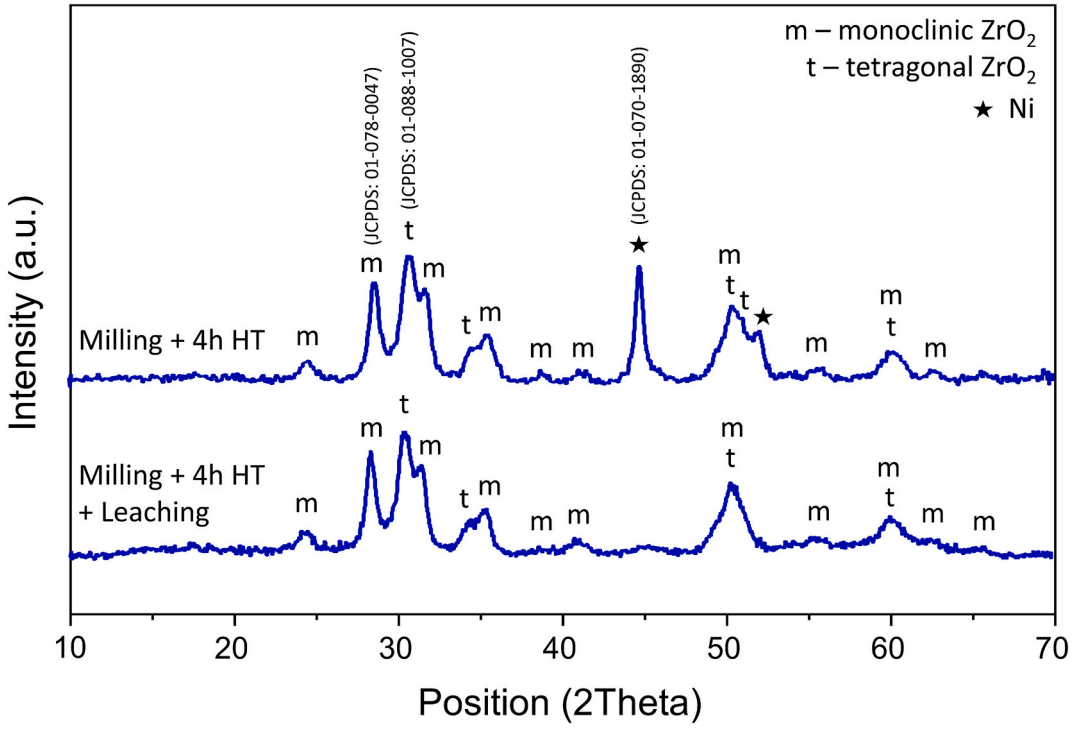

Fig. 9. XRD spectra of milled and hydrothermally-treated EoL Ni-YSZ powders before and after the selective extraction of Ni carried out through HNO_3 acid leaching in batch conditions.

full amount of metallic Ni has been extracted from the Ni-YSZ composite. In addition, based on the specifications provided by the SOC manufacturer, minimal residuals of Ni do not prevent the use of the recycled YSZ for the re-manufacturing cell anode components, since the ceramic phase will be combined with NiO to obtain the composite electrode by thermal sintering.

Negligible amount of detected leaching of Y (7 ppm) and Zr (180 ppm) under the investigated conditions can be ascribed to surface acid-catalysed hydrolysis locally occurring at the YSZ particles. However, this limited surface reactivity at low pH conditions did not result, as shown

Table 3
(a) SSA and PSD of Ni-YSZ powders before and after the selective extraction of Ni through HNO_3 acid leaching; (b) concentrations (ppm) of Ni, Y and Zr evaluated through ICP analysis of the supernatants recovered after leaching and EDS elemental analysis for the evaluation of Ni, Y, Zr, and O atomic concentrations in the powders before (4 h HT) and after acid-assisted leaching (4 h HT + acid-leaching).

(a)

Treatment	Specific Surface Area ($m^2\ g^{-1}$)	Particle Size ± Std. Dev. * (nm)
Milling	8	400 ± 80
Milling +4 h HT	13	380 ± 80
Milling +4 h HT + acid-leaching	17	350 ± 80

(b)

Treatment	ICP Elemental analysis (ppm)			EDS Elemental Analysis (Atomic %)			
	Ni	Y	Zr	Ni	Y	Zr	O
Milling +4 h HT	0.6	ND**	ND**	25.3	1.2	48.5	25.2
Milling +4 h HT + acid-leaching	8×10^3	7	180	0.8	2.5	72.2	29.9

* (derived from distribution % number).
** ND: not detectable.

before, in significant degradation of the crystalline structure, therefore is not expected to negatively affect the quality of the recovered ceramic phase.

At variance, a significant increase of SSA from 13 to 17 $m^2\ g^{-1}$ has been observed (Table 3.b) for acid-treated powder. Since the average particle size resulted somehow unaffected by the treatment, the relevant increase of SSA upon acid leaching is mostly attributed to the removal of nickel from the composite material, where the ceramic and the metallic phase are intimately mixed, resulting in the formation of cavities at the surface of YSZ particles. According to the manufacturer specifications, SSA is considered a key parameter to assure the appropriate sinterability of the composite electrodes and the targeted value (17 $m^2\ g^{-1}$) for the recycled powder perfectly align to the most commonly reported values in the range 12–20 $m^2\ g^{-1}$.

FESEM micrographs of the powders after acid leaching (Fig. 10) did not reveal any substantial change, except for a higher tendency to aggregate, most likely ascribed to larger presence of hydroxyl groups at the particles surface, leading to enhanced intraparticle interactions.

Overall, the efficacy of the investigated Ni extraction approach resulted selective and efficient, leading to a recovered YSZ phase with negligible nickel residues and appropriate structural (crystallinity, SSA) and morphological features (average particle size).

4. Conclusions

To the authors' knowledge so far, no single study has been specifically reported about the recovery of critical raw materials from EoL SOC components. With this perspective, the current study represents a first essential step towards the recovery of valuable electrode materials from SOCs dismantled after long operation time. In particular, a recycling multi-step pathway has been adapted and optimized to separate the Ni-YSZ electrodes from the whole EoL cells and to selectively extract Ni from the metal-ceramic composite, with the purpose of recovering the YSZ ceramic phase, as the main component of the entire cell.

To this aim, a complete process was defined starting from the as-received EoL cells dismantled from stacks to the recovered YSZ powders, aimed at cell electrode re-manufacturing.

Each step of the process was optimized based on the physico-chemical, structural and morphological characterization of the resulting powder. Specifically, cells were first pulverised into powders by a preliminary milling step of 6 h and sieving, that resulted in powders characterised by specific surface area of 8 $m^2\ g^{-1}$ and consisting of submicrometric particles (*ca* 400 nm) and micro-sized aggregates. Hydrothermal (HT) treatment at 200 °C was exploited to further disaggregate the Ni-YSZ composite powders and increase the specific surface

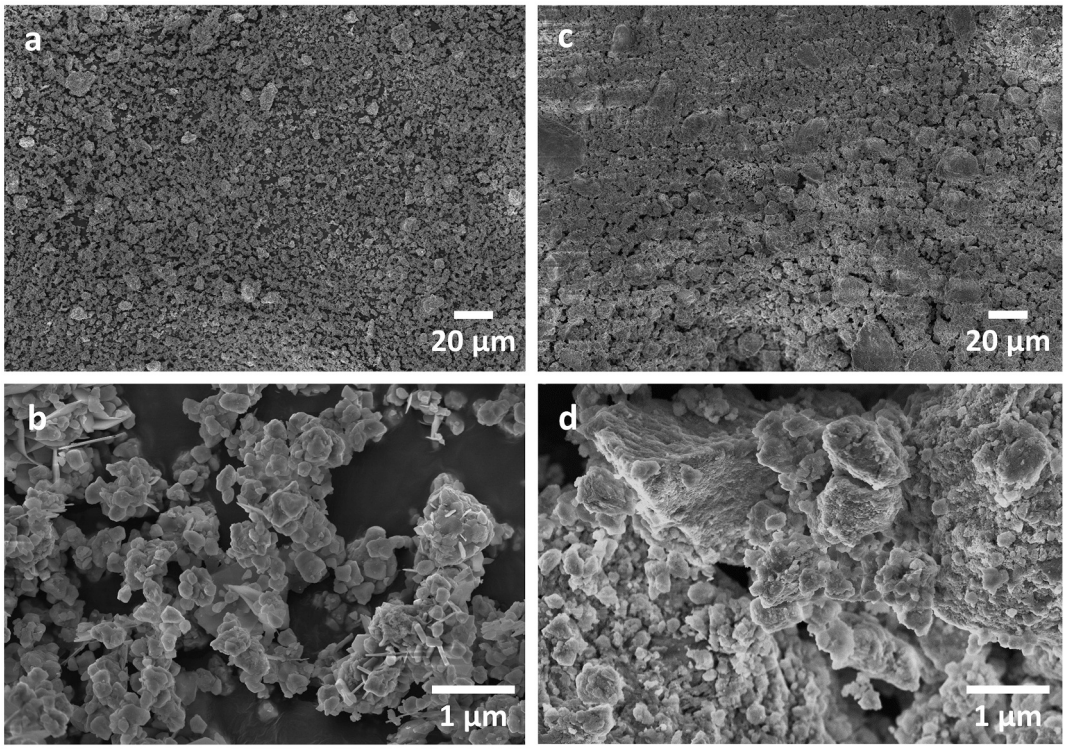

Fig. 10. FESEM morphological characterization of EoL Ni-YSZ powders before (a,b) and after (c,d) HNO_3 acid leaching.

area exposed to enhance the efficacy of the acid-assisted leaching of nickel. HT treatment conducted for 4 h allowed to achieve the best results in terms of surface area increase as well as morphological (particle size distribution) and structural features of the obtained powders, while minimizing the energy consumptions. The selective full extraction of Ni from Ni-YSZ powder was carried out by using an HNO_3 solution at 80 °C for 2 h, which allowed to preserve the YSZ crystallinity and did not induce any substantial loss of the ceramic phase. Minimal nickel residues (0.8% atomic percentage) as evidenced by EDS analysis of the recycled powders are not considered a major drawback in view of reusing the powder for cell remanufacturing, since the ceramic phase will be mixed in appropriate amount with NiO and thermally treated to promote the full densification of the composite electrode.

Based on the literature [35–38], the specific surface area (17 $m^2\ g^{-1}$) and particle size distribution (average particles size of 400 nm) of the recovered YSZ powders meet the specifications of the ceramic powders commonly used for SOC components (electrolyte and electrodes) manufacturing.

According to SOC manufacturer's specifications, the specific surface area and particles size of the ceramic phase are key parameters to assure the appropriate powder sinterability and in turn the electrochemical performance of the electrodes. In conclusions the obtained achievements demonstrate the potential of the developed recovery procedure in providing high-quality recycled materials, with associated reduction of the environmental impact and costs.

Author statement

Sofia Saffirio: Investigation, Writing-Original draft preparation, Methodology; Sergii Pylypko : Conceptualization, Methodology, Validation, Writing- Reviewing and Editing; Sabina Fiorot: Conceptualization, Methodology, Writing- Reviewing and Editing; Ilaria Schiavi: Methodology, Writing- Reviewing and Editing; Silvia Fiore: Methodology, Writing- Reviewing and Editing; Massimo Santarelli: Conceptualization, Methodology, Validation; Domenico Ferrero: Investigation, Methodology, Validation; Federico Smeacetto: Conceptualization, Methodology, Writing- Reviewing and Editing; Sonia Fiorilli: Conceptualization, Methodology, Writing- Reviewing and Editing.

Declaration of Competing Interest

The authors declare that they have no known competing financial interests or personal relationships that could have appeared to influence the work reported in this paper.

Acknowledgments

This project has received funding from the Fuel Cells and Hydrogen 2 Joint Undertaking (now Clean Hydrogen Partnership) under Grant Agreement No 101007216. This Joint Undertaking receives support from the European Union's Horizon 2020 Research and Innovation program, Hydrogen Europe and Hydrogen Europe Research.

Appendix A. Supplementary data

Supplementary data to this article can be found online at https://doi.org/10.1016/j.susmat.2022.e00473.

References

[1] Z. Abdin, A. Zafaranloo, A. Rafiee, W. Mérida, W. Lipiński, K.R. Khalilpour, Hydrogen as an energy vector, Renew. Sust. Energ. Rev. 120 (2020), 109620, https://doi.org/10.1016/J.RSER.2019.109620.

[2] A.M. Abdalla, et al., Nanomaterials for solid oxide fuel cells: a review, Renew. Sust. Energ. Rev. 82 (2018) 353–368, https://doi.org/10.1016/J.RSER.2017.09.046.

[3] D.K. Niakolas, M. Daletou, S.G. Neophytides, C.G. Vayenas, Fuel cells are a commercially viable alternative for the production of "'clean"' energy, Ambio 45 (2016) S32–S37, https://doi.org/10.1007/s13280-015-0731-z.

[4] A. Valente, D. Iribarren, J. Dufour, End of life of fuel cells and hydrogen products: from technologies to strategies, Int. J. Hydrog. Energy 44 (2019) 20965–20977, https://doi.org/10.1016/J.IJHYDENE.2019.01.110.

[5] E.I. Wright, S. Rahimifard, Strategic decision making for end-of-life management of fuel cells, in: Leveraging Technol. A Sustain. World - Proc. 19th CIRP Conf. Life Cycle Eng, 2012, pp. 185–190, https://doi.org/10.1007/978-3-642-29069-5_32.

[6] E. Ivers-Tiffée, A. Weber, D. Herbstritt, Materials and technologies for SOFC-components, J. Eur. Ceram. Soc. 21 (2001) 1805–1811, https://doi.org/10.1016/S0955-2219(01)00120-0.

[7] K. Chen, X. Chen, Z. Lü, N. Ai, X. Huang, W. Su, Performance of an anode-supported SOFC with anode functional layers, Electrochim. Acta 53 (27) (Nov. 2008) 7825–7830, https://doi.org/10.1016/J.ELECTACTA.2008.05.063.

[8] M. Liu, et al., High-performance cathode-supported SOFCs prepared by a single-step co-firing process, J. Power Sources 182 (2008) 585–588, https://doi.org/10.1016/J.JPOWSOUR.2008.04.039.

[9] M.E. Chelmehsara, J. Mahmoudimehr, Techno-economic comparison of anode-supported, cathode-supported, and electrolyte-supported SOFCs, Int. J. Hydrog. Energy 43 (2018) 15521–15530, https://doi.org/10.1016/J.IJHYDENE.2018.06.114.

[10] M. Han, X. Tang, H. Yin, S. Peng, Fabrication, microstructure and properties of a YSZ electrolyte for SOFCs, J. Power Sources 165 (2007) 757–763, https://doi.org/10.1016/J.JPOWSOUR.2006.11.054.

[11] D. Rembelski, J.P. Viricelle, L. Combemale, M. Rieu, Characterization and comparison of different cathode materials for SC-SOFC: LSM, BSCF, SSC, and LSCF, Fuel Cells 12 (2012) 256–264, https://doi.org/10.1002/FUCE.201100064.

[12] H. Uchida, S. Arisaka, M. Watanabe, High performance electrodes for medium-temperature solid oxide fuel cells: activation of La(Sr)CoO3 cathode with highly dispersed Pt metal electrocatalysts, Solid State Ionics 135 (2000) 347–351, https://doi.org/10.1016/S0167-2738(00)00465-3.

[13] C. Jin, C. Yang, F. Chen, Effects on microstructure of NiO–YSZ anode support fabricated by phase-inversion method, J. Membr. Sci. 363 (2010) 250–255, https://doi.org/10.1016/J.MEMSCI.2010.07.044.

[14] A.M. Férriz, A. Bernad, M. Mori, S. Fiorot, End-of-life of fuel cell and hydrogen products: a state of the art, Int. J. Hydrog. Energy 44 (2019) 12872–12879, https://doi.org/10.1016/J.IJHYDENE.2018.09.176.

[15] Report E4tech (UK) Ltd for FCH 2 JU in partnership with Ecorys and Strategic Analysis Inc, Study on Value Chain and Manufacturing Competitiveness Analysis for Hydrogen and Fuel Cells Technologies, FCH contract 192, September 2019.

[16] M. Mori, R. Stropnik, M. Sekavčnik, A. Lotrič, Criticality and life-cycle assessment of materials used in fuel-cell and hydrogen technologies, Sustain. 2021 (13) (2021) 3565, https://doi.org/10.3390/SU13063565.

[17] S. Krishnan, et al., Current technologies for recovery of metals from industrial wastes: an overview, Environ. Technol. Innov. 22 (2021), 101525, https://doi.org/10.1016/J.ETI.2021.101525.

[18] M. Marafi, A. Stanislaus, Waste catalyst utilization: extraction of valuable metals from spent hydroprocessing catalysts by ultrasonic-assisted leaching with acids, Ind. Eng. Chem. Res. 50 (2011) 9495–9501, https://doi.org/10.1021/IE200789U.

[19] E. Young Kim, J. Chun Lee, B.S. Kim, M.S. Kim, J. Jeong, Leaching behavior of nickel from waste multi-layer ceramic capacitors, Hydrometallurgy 86 (2007) 89–95, https://doi.org/10.1016/J.HYDROMET.2006.11.007.

[20] F. Vegliò, R. Quaresima, P. Fornari, S. Ubaldini, Recovery of valuable metals from electronic and galvanic industrial wastes by leaching and electrowinning, Waste Manag. 23 (2003) 245–252, https://doi.org/10.1016/S0956-053X(02)00157-5.

[21] W.S. Chen, H.J. Ho, Recovery of valuable metals from Lithium-ion batteries NMC cathode waste materials by hydrometallurgical methods, Met. 2018 (8) (2018) 321, https://doi.org/10.3390/MET8050321.

[22] J. Lie, Y.C. Lin, J.C. Liu, Process intensification for valuable metals leaching from spent NiMH batteries, Chem. Eng. Process. Process Intensif. 167 (2021), 108507, https://doi.org/10.1016/J.CEP.2021.108507.

[23] A. Fernandes, J.C. Afonso, A.J.B. Dutra, Separation of nickel(II), cobalt(II) and lanthanides from spent Ni-MH batteries by hydrochloric acid leaching, solvent extraction and precipitation, Hydrometallurgy 133 (2013) 37–43, https://doi.org/10.1016/J.HYDROMET.2012.11.017.

[24] V. Innocenzi, F. Vegliò, Recovery of rare earths and base metals from spent nickel-metal hydride batteries by sequential sulphuric acid leaching and selective precipitations, J. Power Sources 211 (2012) 184–191, https://doi.org/10.1016/J.JPOWSOUR.2012.03.064.

[25] I.Y. Kozlowskaya, V.N. Martsul, Acid leaching of lanthanum from spent cracking catalyst, Russ. J. Appl. Chem. 8712 (87) (2014) 1817–1822, https://doi.org/10.1134/S1070427214120040 (2015).

[26] X. Jun Bao, et al., Conversion of cerium and lanthanum from rare earth polishing powder wastes to CeO_2 and $La_{0.6}Ca_{0.4}CoO_3$, Hydrometallurgy 193 (2020), 105317, https://doi.org/10.1016/J.HYDROMET.2020.105317.

[27] C. Sposato, et al., Towards the circular economy of rare earth elements: lanthanum leaching from spent FCC catalyst by acids, Process. 2021 (9) (2021) 1369, https://doi.org/10.3390/PR9081369.

[28] M. Kamiya, Y. Mori, T. Kojima, R. Sasai, H. Itoh, Recycling process for yttria-stabilized tetragonal zirconia ceramics using a hydrothermal treatment, J. Mat. Cycles Waste Manag. 9 (2007) 27–33, https://doi.org/10.1007/s10163-006-0168-3.

[29] H. Kim, C. Da Rosa, M. Boaro, J.M. Vohs, R.J. Gorte, Fabrication of highly porous yttria-stabilized zirconia by acid leaching nickel from a nickel-yttria-stabilized

zirconia cermet, J. Am. Ceram. Soc. 85 (2002) 1473–1476, https://doi.org/10.1111/J.1151-2916.2002.TB00299.X.
[30] N. Mketoa, P.N. Nomngongoa, J.C. Ngila, A rapid microwave-assisted acid extraction method based on the use of diluted HNO_3-H_2O_2 followed by ICP-MS analysis for simultaneous determination of trace elements in coal samples, Int. J. Environ. Anal. Chem. 95 (2015) 453–465, https://doi.org/10.1080/03067319.2015.1025226.
[31] T. Götsch, W. Wallisch, M. Stöger-Pollach, B. Klötzer, S. Penner, From zirconia to Yttria: sampling the YSZ phase diagram using sputter-deposited thin films, AIP Adv. 6 (2016), 025119, https://doi.org/10.1063/1.4942818.
[32] L.M. Candido, L.M.G. Fais, E.B. Ferreira, S.G. Antonio, L.A.P. Pinelli, Characterization of a diamond ground Y-TZP and reversion of the tetragonal to monoclinic transformation, Oper. Dent. 42 (2017) 407–417, https://doi.org/10.2341/16-196-L.
[33] C. Areeprasert, D. Ma, P. Prayoga, K. Yoshikawa, A review on pilot-scale applications of hydrothermal treatment for upgrading waste materials, Int. J. Env. Sci. Dev. 7 (2016) 425–430.
[34] T. Kojima, Y. Mori, M. Kamiya, R. Sasai, H. Itoh, Disintegration process of yttria-stabilized zirconia ceramics using hydrothermal conditions, J. Mater. Sci. 42 (2007) 6056–6061, https://doi.org/10.1007/s10853-006-1167-4.
[35] T. Baquero, J. Escobar, J. Frade, Dachamir Hotza, Aqueous tape casting of micro and nano YSZ for SOFC electrolytes, Ceram. Int. 39 (2013) 8279–8285, https://doi.org/10.1016/j.ceramint.2013.03.097.
[36] S.T. Aruna, M. Muthuraman, K.C. Patil, Synthesis and properties of Ni-YSZ cermet: anode material for solide oxide fuel cells, Solid State Ionics 111 (1998), 45–41.
[37] J.H. Jang, J.H. Ryu, S.M. Oh, Microstructure of Ni/YSZ cermets according to particle size of precursor powder and their anodic performances in SOFC, Ionics 6 (2000) 86–91.
[38] W.K. Yoshito, V. Ussui, D.R.R. Lazar, J.O.A. Paschoal, Synthesis and characterization of NiO-8YSZ powders by coprecipitation route, Mater. Sci. Forum 498-499 (2005) 612–617, https://doi.org/10.4028/www.scientific.net/MSF.498-499.612.